DOI:
10.1109/TAP.2017.2679067

Document Version
Peer reviewed version

Multiple-frequency DBIM-TwIST algorithm for microwave breast imaging

Zhenzhuang Miao and Panagiotis Kosmas, Senior Member, IEEE

***Abstract*—A novel DBIM algorithm is proposed for microwave breast imaging based on the TwIST method. We show that this implementation is more flexible and robust than using traditional Krylov subspace methods such as the CGLS as solvers of the ill-posed linear problem. The paper presents several strategies to increase the algorithm's robustness: a hybrid multi-frequency approach to achieve an optimal trade-off between imaging accuracy and reconstruction stability; a new approach to estimate the average breast tissues properties, based on sampling along their range of possible values and running a few DBIM iterations to find the minimum error; and finally, a new regularization strategy for the DBIM method based on the L^1 norm and the Pareto curve. We present reconstruction examples which illustrate the benefits of these optimization strategies, which have resulted in a DBIM algorithm that outperforms our previous implementations for microwave breast imaging.**

***Index Terms*—Microwave breast imaging, DBIM, TwIST, multiple-frequency, hybrid frequency, multiple-resolution, initial guess, L^1 norm regularization method.**

I. Introduction

Microwave tomographic methods for medical imaging estimate the spatial distribution of dielectric properties in a tissue region by solving an electromagnetic (EM) inverse scattering problem [1], [2]. Various EM inverse scattering methods have been proposed in recent years for this purpose, such as conjugate gradient techniques [3], [4] and Gauss-Newton (GN) optimization algorithms [5]. In our previous work, we have applied a Gauss-Newton (GN) algorithm based on the distorted Born iterative method (DBIM), which approximates the nonlinear inverse scattering problem by an under-determined set of linear equations [6], [7]. Moreover, we have applied adaptive thresholding methods to solve this set of linear equations thereby improving reconstructions in DBIM-based microwave breast imaging [8].

More recently, we have shown that the use of the two-step iterative shrinkage/thresholding method (TwIST) [9] can further improve the solution of the ill-posed linear system in microwave breast imaging [10]. By using two previous iterates to compute the current update of the iterative linear solver, the TwIST algorithm can lead to faster convergence and more accurate reconstructions compared to conventional adaptive thresholding methods [10]. In addition, the algorithm provides a set of flexible parameters that can increase robustness relative to one-step iterative methods.

This paper presents new strategies which improve further the performance of the DBIM-TwIST algorithm for microwave breast imaging. First, we present a two-step reconstruction approach, where the first step considers a homogeneous breast interior and uses the DBIM to obtain an initial guess which reflects the true breast tissue composition. This step is critical for the DBIM to converge to an optimal solution (global minimum), as GN algorithms can be very sensitive to the initial guess in applications such as medical imaging, where very little a *priori* information may be available [11], [12]. In particular, an initial guess provides the starting point for these convex optimization algorithms, and inaccurate information can lead to false solutions that fit the data but are completely different from the ground truth [13]. Our approach adds low computational cost to the final breast reconstructions, and improves significantly the reconstruction quality for different breast phantoms.

Moreover, we improve the performance of the DBIM-TwIST further by refining our previous work on multiple-frequency reconstructions using a single-pole Debye model [8], [10]. Reconstructing the single-pole Debye parameters allows multiple frequency data to be used for the inversion at each DBIM iteration [2], [6], [8]. Multiple-frequency approaches can combine the stabilizing effects of lower frequencies with enhanced resolution of higher frequencies, thereby overcoming stability and resolution limitations of single-frequency algorithms which tend to be very dependent upon the chosen frequency [14].

Our analysis provides insight on how to utilize multiple-frequency information to enhance the accuracy of reconstruction and robustness of the DBIM-TwIST algorithm. Our adopted hybrid frequency approach provides better stability and reconstruction accuracy at lower computational cost relative to frequency-hopping techniques [4]. We also confirm the intuitive result that the optimal initial guess obtained in the first step of our algorithm requires only low-frequency data, which can be obtained using a low resolution grid.

Finally, we present a new method for regularizing the unconstrained optimization problem based on L^1 norm minimization and the TwIST method. This is motivated by recent work in medical applications, where regularization methods based on the L^1 norm or total variation (TV) principle have become popular instead of L^2 norm regularization approaches [15]. These methods impose less smoothing on the reconstruction image. In this paper we implement the Pareto curve for finding the L^1 norm regularization parameter of the TwIST algorithm, which defines the optimal trade-off between the L^2 norm of the residual and the L^1 norm of the solution [16]. The non-stationary convergence of the TwIST method does not ensure differentiability and continuity of the Pareto curve, as in stationary iterative methods such as conjugate gradient method. We therefore employ curve fitting of cubic polynomials to smooth the Pareto curve. Moreover, we apply

an exponential distribution sampling of the regularization parameter to reduce computation cost.

These new strategies, which are presented in a unified framework within the DBIM, provide some unique capabilities of our algorithm relative to recently proposed alternative methods. For example, Nikolova et al in [17], [18], presented an interesting and effective holography method for reconstructing targets in the near-field range, which relies on an alternative formulation of the problem. Similarly, theoretical and experimental work by LoVetri et al has also focused on two-dimensional (2-D) wideband microwave imaging using various approaches including the DBIM [19], but the employed optimization and regularization strategies are very different from this work. Moreover, the importance of the initial guess in the convergence of the algorithm has been demonstrated in numerous papers (see for example [11]), but the approach presented here to tackle this problem has not been considered previously, to the best of our knowledge.

The remainder of this paper is structured as follows. Section II presents several implementation aspects of our DBIM-TwIST algorithm for microwave breast imaging, while Section III introduces our new inversion strategies to enhance inversion. Section IV presents simulation results to illustrate the advantages of our algorithm, and some final conclusions are given in Section V.

II. Implementation of the DBIM-TwIST algorithm

A. Review of the DBIM-TwIST algorithm

The DBIM is an iterative inverse scattering algorithm which is commonly used to estimate the spatial distribution of dielectric properties within a region V [20]. Under the Born approximation, a linear integral equation at each iteration can be discretized for all transmit-receive pairs, leading to a linear system that can be solved by various methods including the TwIST method, as presented in our previous work [10].

In particular, the TwIST algorithm [9] can be introduced by considering the linear system at each DBIM iteration as an inverse problem where the goal is to estimate an unknown original image vector x from an observation vector y, described by the linear equation $A\boldsymbol{x} = \boldsymbol{y}$. Many approaches to this *Linear Inverse Problem* (LIP) define a solution $\hat{\boldsymbol{x}}$ as a minimizer of a convex objective function $f : \chi \rightarrow R = [-\infty, +\infty]$, given by

$$f(\boldsymbol{x}) = \frac{1}{2}\|\boldsymbol{y} - A\boldsymbol{x}\|_2^2 + \lambda\Phi(\boldsymbol{x}) \tag{1}$$

where $\Phi(\boldsymbol{x})$ is a regularization function for the convex optimization problem and $\lambda \in [0, +\infty]$ is a weighting parameter. Note that we use a standard definition for the norm through the paper given by $\|\cdot\|_p = \sqrt{(\sum_n |\cdot|^p)}$.

In recent years, iterative algorithms were independently proposed by many authors within different frameworks, e.g. [9], [21]–[24]. Our implementation is based on [9], which presents a method of splitting the matrix to structure a two-step iterative equation shown below:

$$\begin{aligned} \boldsymbol{x}_{t+1} &= (1-\alpha)\boldsymbol{x}_{t-1} + (\alpha-\beta)\boldsymbol{x}_t + \beta\Gamma_\lambda(\boldsymbol{x}_t) \\ \Gamma_\lambda(\boldsymbol{x}) &= \Psi_\lambda(\boldsymbol{x} + A^T(\boldsymbol{y} - A\boldsymbol{x})) \end{aligned} \tag{2}$$

where α and β are the parameters of the TwIST algorithm, and Ψ_λ is the denoising function corresponding to the regularization function Φ [3]. The designation two-step stems from the fact that the next estimate $\boldsymbol{x}_{t+1}$ depends on both the current solution $\boldsymbol{x}_t$ and the previous solution $\boldsymbol{x}_{t-1}$, rather than only on $\boldsymbol{x}_t$, as in conventional iterative shrinkage thresholding algorithms.

In our previous paper [10], we have presented a methodology to increase the robustness of the DBIM-TwIST algorithm, as well as ways to optimise its parameters for a particular application such as microwave breast imaging. This robustness is an important advantage of the TwIST method relative to other iterative solvers such as CGLS, as suggested by our comparison results in Section IV-A.

B. Testbeds

We consider a 2-D microwave breast imaging simulation scenario that has been used in previous work to evaluate imaging performance with different inversion approaches [8], [25]. Simulation data is produced with the FDTD method with a CPML boundary condition. Our tests include all four types of numerical breast phantoms taken from the UWCEM repository [26]. In particular, we have considered 2-D axial slices representative of the phantoms classified as 'mostly fatty' (ID:071904), 'scattered fibroglandular' (ID:010204), 'heterogeneously dense' (ID:062204) and 'very dense' (ID:010204). The single-pole Debye model is employed to describe the frequency-dependence for all breast tissues in the computation model,

$$\epsilon_r(\omega) = \epsilon_\infty + \frac{\epsilon_s - \epsilon_\infty}{1 + j\omega\tau} - j\frac{\sigma_s}{\omega\epsilon_0} \tag{3}$$

where τ is assumed constant for all tissues (with a value of 17.125 ps). As in previous work [2], [8], [10], we assume a lossless background medium with $\epsilon_r = 2.6$ in our simulations, but we examine the impact of losses for some realistic background coupling media in Section IV-D. Our setup considers sixteen antennas surrounding the 2-D breast phantom, representing point sources excited with a wideband Gaussian pulse in a TM configuration (i.e. the electric field is perpendicular to the breast phantom). Six sampling frequencies are selected at 1.0, 1.5, 2.0, 2.5, 3.0, and 3.5 GHz.

We note that the choice for the number of antennas is based on the analysis in [27]. In the 2-D scalar case, the essential number of the antennas is defined as,

$$M = 2\beta\alpha \tag{4}$$

where α is the radius of the reconstruction domain and β is the wave number. Considering our first operating frequency of 1 GHz, M is approximately equal to 15.

The shape of breast model is the only prior information assumed known for the reconstruction, while the relative dielectric permittivity of the skin and its thickness are unknown.

To compare image reconstruction quality, we define a relative reconstruction error as,

$$\text{"}Relative\ error\text{"} = \frac{\|\epsilon^t_{\infty original} - \epsilon^t_{\infty reconstructed}\|^2}{\|\epsilon^t_{\infty orginal}\|^2}, \tag{5}$$

where t is the iteration number and $\|\cdot\|$ denotes the L^2 norm in this paper. In (5), ϵ_∞ is chosen as the representative of reconstructed Debye parameter, but similar metrics can be calculated for any of the parameters of the Debye (or an Ohmic) model.

As we cannot know the true ϵ_∞ in a realistic application, we must also define a "Residual" error as,

$$Residual = \|M_t^E - M_t^S\| \tag{6}$$

where M_t^E and M_t^S denote complex vectors of the "experimental" and "model" data at the t_{th} iteration respectively, recorded at the antenna locations. The "Residual" difference can be computed at each DBIM iteration, and can be used as a stopping criterion for the DBIM iterative algorithm.

C. FDTD implementation in multiple grid resolutions

Our work investigates imaging performance for different voxel sizes, in order to assess our DBIM-TwIST algorithm's resolution limitations. The resolution of our original breast models is 0.5 mm, so we propose to reconstruct images in four different grid resolutions, i.e. 2 mm, 1.5 mm, 1 mm, and 0.5 mm. We note that the maximum resolution must be smaller than the thickness of the skin. Consequently, 2 mm is the maximum for the multi-resolution implementation based on our original breast model.

Naturally, the choice of the grid resolution affects the numerical data mismatch error of our FDTD forward solver. In particular, the FDTD simulation data sampling frequency depends on the inverse of the FDTD time-step Δt which is fixed relative to the spatial increment $\Delta x = \Delta y$ according to Courrant's criterion to avoid numerical instability, e.g.,

$$\Delta t = \Delta x/(2 * c) \tag{7}$$

where c denotes the speed of light in vacuum. We apply a soft source excitation, which commonly uses a current source as a drive to produce a required field, such as

$$\boldsymbol{E}_{n+1} = \boldsymbol{E}_n + source(n) \tag{8}$$

where $source(n)$ is a discrete series of the voltage source. This soft source causes successive accumulations of energy for different time-step Δt. To tackle the problem, we must amend the relationship between Δx and Δt and modify the amplitude of simulated source to compensate for this error as we move from the 0.5 mm grid to its multiple increments 1.0, 1.5, and 2.0. We therefore define a parameter mul as the ratio of the multiple resolution to the 'original' resolution grid of 0.5 mm, as shown below,

$$\begin{aligned} mul &= r_c/0.5mm \\ \Delta t &= \Delta x/(2 * c)/mul \\ source_m &= source_o/mul^2 \end{aligned} \tag{9}$$

where r_c denotes the targeted resolution, and $source_o$ and $source_m$ are the original excitation signal and the modified source respectively.

Fig. 1 plots the relative errors of received signals from 120 antenna pairs (for the 16 antenna system) in 2.0, 1.5, and 1.0 mm grid resolutions against the received signal in 0.5 mm. The average of relative errors are 0.0725, 0.0422, and 0.0251 respectively. It is evident that the targeted resolution closer to the fine original model in 0.5 mm results in the least relative error. In all cases, our compensation method results in a data mismatch under 8% relative to the original numerical phantom. This data mismatch due to the forward solver's numerical discretization is negligible relative to the model mismatch between the true numerical phantom and our initial guess of a homogeneous breast interior with unknown skin properties.

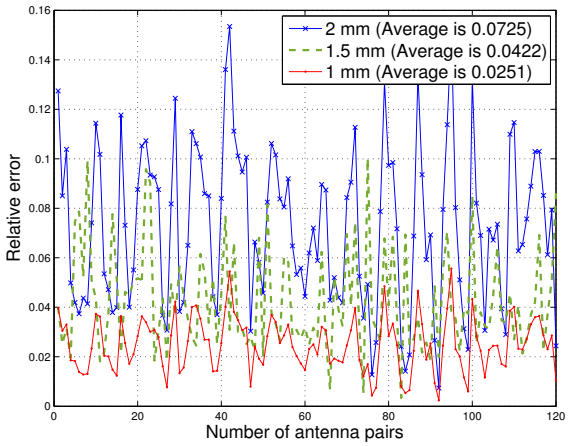

Fig. 1. Errors of FDTD-calculated signals at the receiver points for multiple grid resolutions against the 0.5 mm resolution of the original phantom.

III. Techniques to optimize convergence

This section discusses implementation strategies to improve the DBIM-TwIST algorithm in terms of robustness and resolution. First, we propose a simple method to estimate the optimal average Debye parameters of the breast, which are then used as the initial guess for the the second step of our reconstruction process. We argue that this optimal initial guess can be obtained from a reconstruction in low resolution, which implies lower computational cost. We then discuss how to best use multi-frequency data to enhance the algorithm's performance. Finally, we propose an L^1 norm regularization of the TwIST method based on the Pareto curve.

A. Optimized initial guess of the breast average dielectric properties

Iterative local optimization methods such as the DBIM method are sensitive to the adopted 'initial guess' of the reconstruction domain [11], which can result in the convex optimization algorithm converging to a false solution. In addition to increasing stability, a good initial guess can speed up convergence, and thus reduce computational time. Obtaining an accurate initial guess can be challenging in applications such as breast imaging, where very little information (e.g. the breast surface) may be known a priori. To this end, we propose a very simple process to estimate the average breast dielectric properties, which relies on the following: 1) assume the breast is homogeneous and filled with normal tissue, and run the

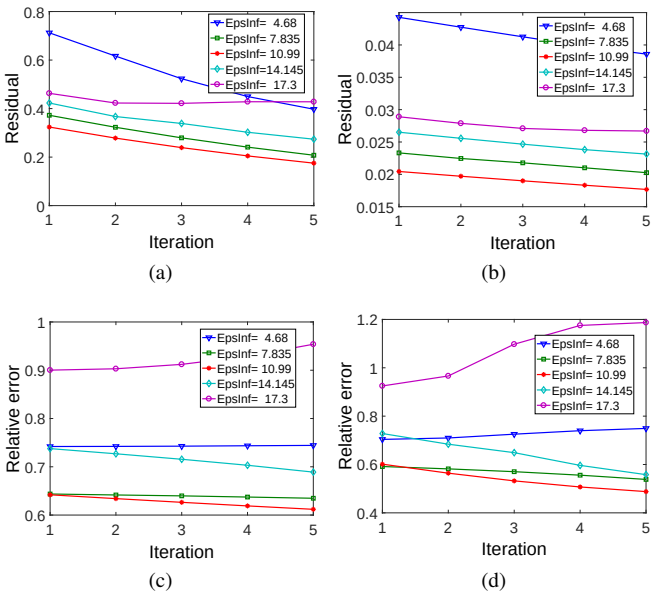

Fig. 2. Illustration of the proposed method to select an optimal initial guess for microwave breast imaging. Here we consider 5 samples from the normal breast tissue range shown in Table I. Each sample is used as the starting point of DBIM-TwIST, which is run for 5 iterations for a fixed a homogeneous breast with unknown skin properties. The residual and relative reconstruction errors vs. iteration number are plotted in (a) and (c) for 2 mm resolution, and in (b) and (d) for 0.5 mm.

DBIM-TwIST algorithm for a fixed number of iterations; 2) apply this process to a number of samples (which we term 'Cases') within a well-known range of values for normal breast tissue to determine the optimal initial guess of the average breast dielectric properties, based on minimizing the data residual.

TABLE I
FIVE CASES OF ESTIMATED INITIAL GUESSES BASED ON THE SINGLE-POLE DEBYE MODEL

Sampling	ϵ_∞	$\Delta\epsilon$	$\sigma_s(S/m)$	$\tau(ps)$
Case 1	4.68	3.21	0.088	17.125
Case 2	7.835	7.26	0.2	17.125
Case 3	10.99	11.3	0.311	17.125
Case 4	14.145	15.35	0.423	17.125
Case 5	17.3	19.4	0.535	17.125

As an example of implementing this approach, we choose 5 samples of the three Debye parameters which are evenly spaced within the range used to model normal breast tissue shown in Table I ('Cases' 1-5), where the parameters of the Case 1 and 5 represent the mean of adipose breast tissue and fibroglandular breast tissue respectively [6]. Then we run 5 iterations of the DBIM-TwIST for each of the 5 cases to select the initial guess with the smallest data residual. This process yields the three Debye parameters of the homogeneous breast interior which reflect the closest estimate to its average dielectric properties and are used as the optimal initial guess in the second step of the DBIM algorithm, to estimate the inhomogeneous breast structure.

Fig. 2 illustrates the evolution of this process for a heterogeneously dense phantom based on a single-frequency reconstruction at 1 GHz. The data residuals and relative reconstruction errors against the original model are plotted at each DBIM iteration for reconstruction resolution of 2 mm in (a) and (c), and 0.5 mm in (b) and (d). The residual and relative errors exhibit similar trends for all cases. Moreover, the similarity of the results in 2 mm and 0.5 mm confirm that it is sufficient to use a 2 mm resolution grid for optimizing the initial guess in this first step of the algorithm even if the final (heterogeneous) images are reconstructed in higher resolutions.

TABLE II
SEVEN RECIPES OF HYBRID FREQUENCY APPROACHES

Name	Hopping method (*iteration No.*)
Freq hopping approach	1→1.5→2→2.5→3→3.5 GHz
Hybrid freq approach 1	1 (20)→ 1.5 + 2 + 2.5 + 3 + 3.5 GHz
Hybrid freq approach 2	1 + 1.5 (20)→ 2 + 2.5 + 3 + 3.5 GHz
Hybrid freq approach 3	1 + 1.5 + 2 (20)→ 2.5 + 3 + 3.5 GHz
Hybrid freq approach 4	1 + 1.5 + 2 + 2.5 (20)→ 3 + 3.5 GHz
Hybrid freq approach 5	1 + 1.5 + 2 + 2.5 + 3 (20)→ 3.5 GHz
Multi-freq approach	1 + 1.5 + 2 + 2.5 + 3 + 3.5 GHz (90)

B. Multiple-frequency optimization

Our recent DBIM-based work has demonstrated that the combination of multi-frequency information can enhance performance in terms of both robustness and resolution [8], [10]. A multi-frequency approach requires a proper dispersion model which should be chosen carefully to reflect true breast tissue dependencies within a frequency range of interest. This work adopts the previously well-established assumption that the single-pole Debye model in (3) can cover the range of 1.0-3.5 GHz [2], [6], [26], thereby allowing us to combine multi-frequency data to estimate the unknown Debye parameters in this entire range.

An alternative method for the use of multi-frequency data is based on the frequency hopping approach, where single-frequency reconstructions are performed successively from low to high frequencies [20]. With this approach, the use of low frequencies in the initial inversion stages reduces the nonlinearity of the problem and increases robustness. However, we have argued in previous work that the method may not take full advantage of high frequency data due to a possibly low rank of the monochromatic linear equation [25].

To balance between these two approaches, we have tested a variety of hybrid frequency approaches with the DBIM-TwIST algorithm, which are listed in Table II. The hybrid approaches rely on using first one or more of the lowest frequencies from our set to provide a crude initial estimate of the breast distribution, which is then used as the starting point for a second DBIM inversion using multi-frequency data from the remaining frequencies. Note here that the low frequency reconstruction is initialized with the output of the algorithm's first step, which provides the optimized initial guess in terms of the breast average dielectric properties (see Section III-A).

Relative reconstruction errors for all seven approaches and the four breast phantoms are shown in Fig. 3. Here we used 15 iterations per frequency for the frequency hopping approach while the hybrid approaches processes the low frequencies in the first 20 iterations, followed by 70 iterations using data

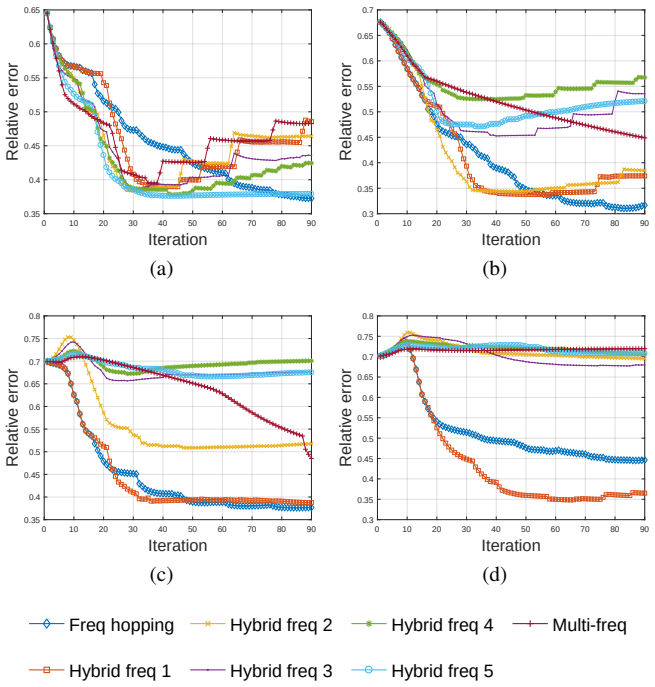

Fig. 3. Relative reconstruction errors for seven multi-frequency approaches in the DBIM-TwIST applied to four breast phantoms with unknown skin properties; (a) in Class 1 for 'mostly fatty'; (b) in Class 2 'scattered fibroglandular'; (c) in Class 3 for 'heterogeneously dense'; (d) in Class 4 for 'very dense'.

from the rest of frequencies. It is evident that the frequency hopping approach and the first hybrid frequency approach are the most stable, while other hybrid frequency approaches are not guaranteed to converge to a minimum. Moreover, the hybrid frequency method is much faster than frequency hopping, requiring between 40 and 60 iterations to converge in all cases.

C. L^1 norm regularization with the TwIST method

Thresholding algorithms such as the TwIST promote sparse solutions of the LIP. We can therefore regularize the TwIST using tools employed by other sparse-promoting algorithms, such as the basis pursuit (BP) problem. BP aims to find a sparse solution of the under-determined system of equations $Ax = b$, where A is an m-by-n matrix and b is m-by-1 vector. Again, if $m << n$, this problem is ill-posed. The approach introduced by Chen, Donoho, and Saunders [28], is to solve the convex optimization problem,

$$\min_x \|x\|_1 \quad \text{subject to} \quad Ax = b. \tag{10}$$

However, it is undesirable to fit exactly the linear system because of noisy or imperfect data. Therefore, other possible formulations of the L^1 norm regularized least-squares problem have been proposed based on the penalized least-squares problem

$$\min_x \quad \|Ax - b\|_2^2 + \lambda\|x\|_1, \tag{11}$$

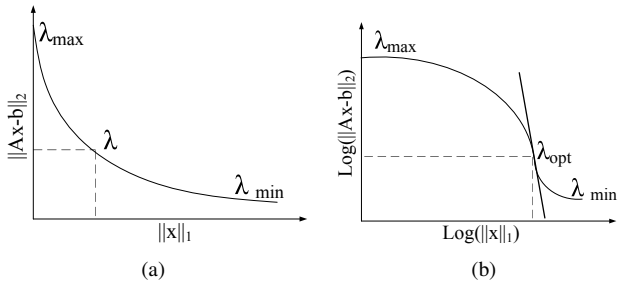

Fig. 4. A typical Pareto curve (a) and Pareto curve in log-log scale (b), which is used to choose the optimal value of the L^1-regularization parameter λ

which is proposed by Chen, Donoho, and Saunders [28], and an explicit L^1 norm constraint problem known as the Lasso problem,

$$\min_x \quad \|Ax - b\|_2 \quad \text{subject to} \quad \|x\|_1 \leq \tau. \tag{12}$$

The formulation of (11) is well suited to the TwIST method because of its close connection to convex quadratic programming, for which we can obtain an explicit expression of the denoising function in closed form. Let x_λ denote the optimal solution of (11). The residual function

$$\phi(\lambda) = \|Ax_\lambda - b\|_2 \tag{13}$$

gives the minimal residual of (11) for each $\lambda \geq 0$.

To obtain the optimal value of λ for $\Phi(\lambda)$, we employ the Pareto curve, which can yield the optimal trade-off between minimizing the L^2 norm of the residual r and the L^1 norm of the solution x, as shown in Fig. 4 for a typical LIP. As the TwIST method is a non-stationary method, the function of (13) is not strictly non-increasing and not smooth. We therefore apply curve fitting using cubic polynomials to approximate the function and its derivative. The curve then becomes continuously differentiable and convex, and the residual ϕ will decrease as λ increases.

Subsequently, we use a log-log scale to plot the norm of residual ϕ on the abscissa against the L^1 norm of solution x for the parameter λ. Then, we can localize a point λ_{opt} corresponding to the maximum of the curve slope. As shown in Fig. 4b, the smallest increase in $\|x\|$ leads to the greatest decrease in $\phi(\lambda)$ around this point. This process is similar to using the L-curve method for L^2 norm regularization problems [29]. However, the L-curve in log-log scale is a convex downward, but the Pareto curve in log-log scale is a convex upward (even if the original Pareto curve is convex downward).

To reduce the computation cost, we choose the value of λ based on an exponentially decreasing function from $\|A^T b\|_\infty$ to zero, which is defined as,

$$\lambda(n) = \|A^T b\|_\infty \cdot \delta^n \qquad n \in \mathbf{Z}^+ \tag{14}$$

where δ denotes a decreasing factor with $0.1 < \delta < 1$, $(\cdot)^T$ denotes a transpose operator, and $\|\cdot\|_\infty$ denotes the infinity norm. In (14), we use δ to control the number of samples for the parameter λ. When δ tends to 1, a more accurate Pareto curve is obtained at the expense of very high computational cost. Conversely, the number of samples becomes insufficient as δ approaches 0.1. In our numerical experiment, a reliable

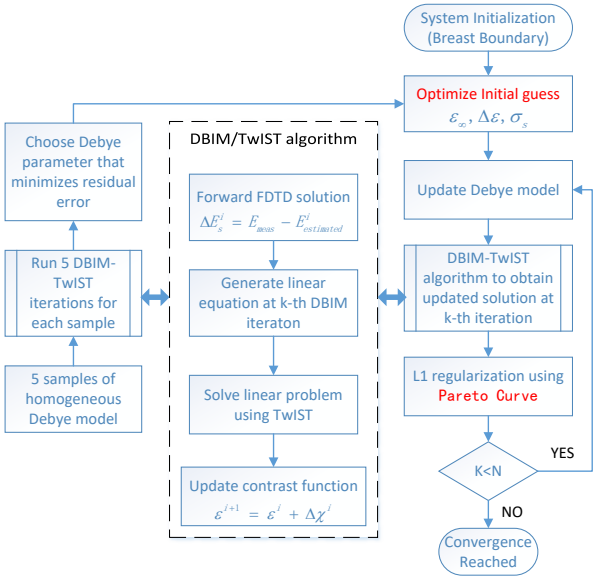

Fig. 5. Flow chart of the multi-frequency DBIM-TwIST algorithm

range of δ is found between 0.3 and 0.5, and any choice in this range comes with a low computational cost.

Finally, it is important to emphasize that, contrary to commonly used L^1 norm approaches, our method combines the Pareto curve with an adaptive strategy to optimize the L^1 regularization based on the residuals of the TwIST iterations at each DBIM iteration, which has been detailed in [10].

IV. Reconstruction Results

For all our results, our reconstruction approach employed the DBIM-TwIST algorithm in conjunction with the optimization strategies presented in Section III as illustrated in Fig. 5. The DBIM-TwIST algorithm is invoked both in the first step of finding the optimal initial guess (average breast properties) as well as in the main reconstruction of the inhomogeneous breast structure. A single frequency approach at 1 GHz is used in the first step, and its outcome initializes the optimal multi-frequency approach (hybrid freq. approach 1 in Table II) employed in the second step of the process.

A. Comparison between TwIST and CGLS

First, we demonstrate that using the TwIST method to solve the LIP can increase the robustness of the DBIM algorithm relative to commonly used CGLS solvers [2], [6]. To this end, we have tested the DBIM with the TwIST and the CGLS in various resolutions, using the frequency hopping approach (in order to examine the impact of each frequency separately). Results are shown in Fig. 6, where it is evident that the TwIST and CGLS methods can provide very similar reconstruction results in resolution of 2 mm, with an almost identical convergence rate. However, for higher resolutions of 1 mm where ill-posedness increases, the CGLS algorithm becomes unstable and converges to a false solution, as shown in Fig. 6 (a) and (c).

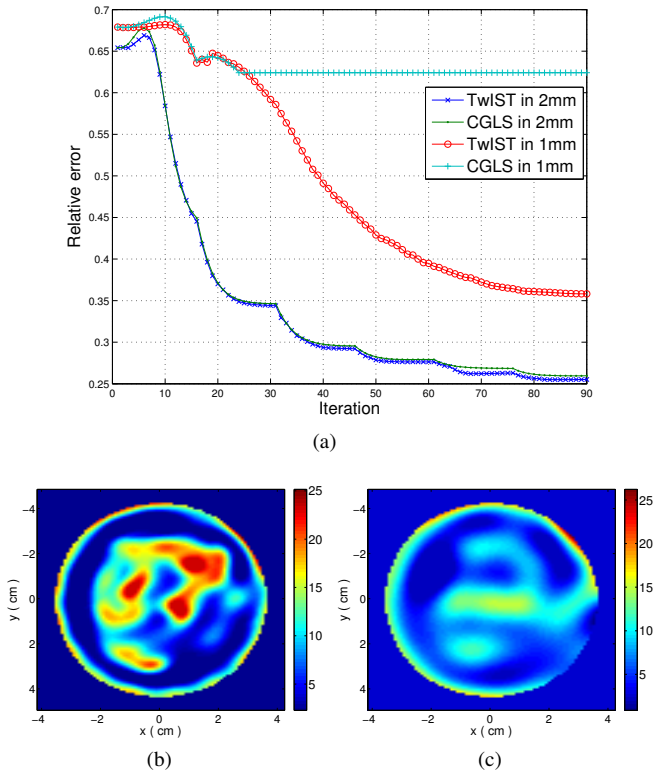

Fig. 6. Comparison between the TwIST algorithm and CGLS algorithm in different resolutions. (a) Relative error of reconstructions based on the frequency hopping approach in 1 mm and 2 mm; (b) Reconstructed image of ϵ_∞ by the TwIST algorithm in 1 mm; (c) Reconstructed image of ϵ_∞ by the CGLS algorithm in 1 mm.

TABLE III
Relative error of reconstructions of ϵ_∞

Model	Default initial guess / Optimized initial guess			
	2 mm	1.5 mm	1 mm	0.5 mm
Class 1	0.264/0.272	0.289/0.301	0.332/0.335	0.429/0.417
Class 2	0.233/0.241	0.266/0.265	0.320/0.297	0.554/0.373
Class 3	0.306/0.312	0.342/0.319	0.380/0.298	0.682/0.361
Class 4	0.473/0.235	0.504/0.261	0.694/0.268	0.707/0.332

This is based on the default initial guess and the optimal initial guess for 4 breast phantoms, including mostly fatty, scattered fibroglandular, heterogeneously dense and very dense breasts from Class 1 to Class 4.

B. Effect of optimizing the initial guess by estimating the breast average dielectric properties

To illustrate the advantage of optimizing the initial guess for the breast average dielectric properties in the DBIM, we have reconstructed axial slices from four UWCEM breast phantoms in resolutions of 2 mm, 1.5 mm, 1 mm, and 0.5 mm. The reconstructed images of ϵ_∞ using a fixed initial guess versus an optimized initial guess in 2 mm and 0.5 mm are shown in Fig. 7 and Fig. 8, respectively. Relative errors computed for the same parameter are given in Table III. Note that the fixed initial guess values are chosen in the middle of the range for the Debye parameters of normal breast tissue.

These images and error values suggest that optimizing the initial guess leads to sufficiently accurate distribution estimates for all resolution ranges, while omitting this step can compromise imaging performance. This is particularly true in all resolution grids for the very dense breast phantom, where

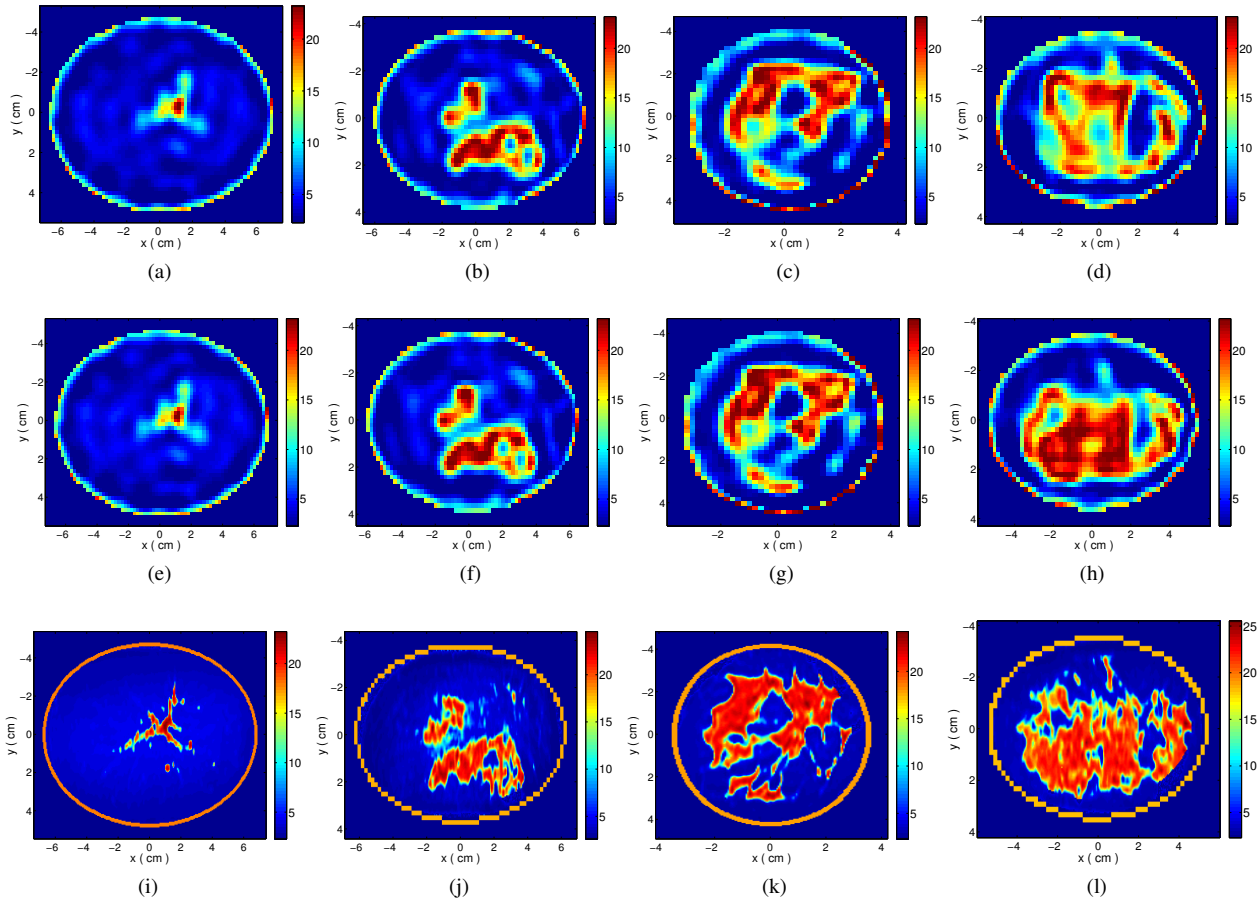

Fig. 7. Reconstructed images of ϵ_∞ without and with optimization of initial guess for 4 phantoms in 2 mm. (a)-(d) Reconstructions with a fixed initial guess representative of normal breast tissue average properties ($\epsilon_\infty = 11.27, \Delta\epsilon = 5.51, \sigma_s = 0.0802$); (e)-(h) Reconstructions with an optimized initial guess; (i)-(l) original 2-D images of 4 breast phantoms (mostly Fatty, scattered fibroglandular, heterogeneously dense and very dense from left to right).

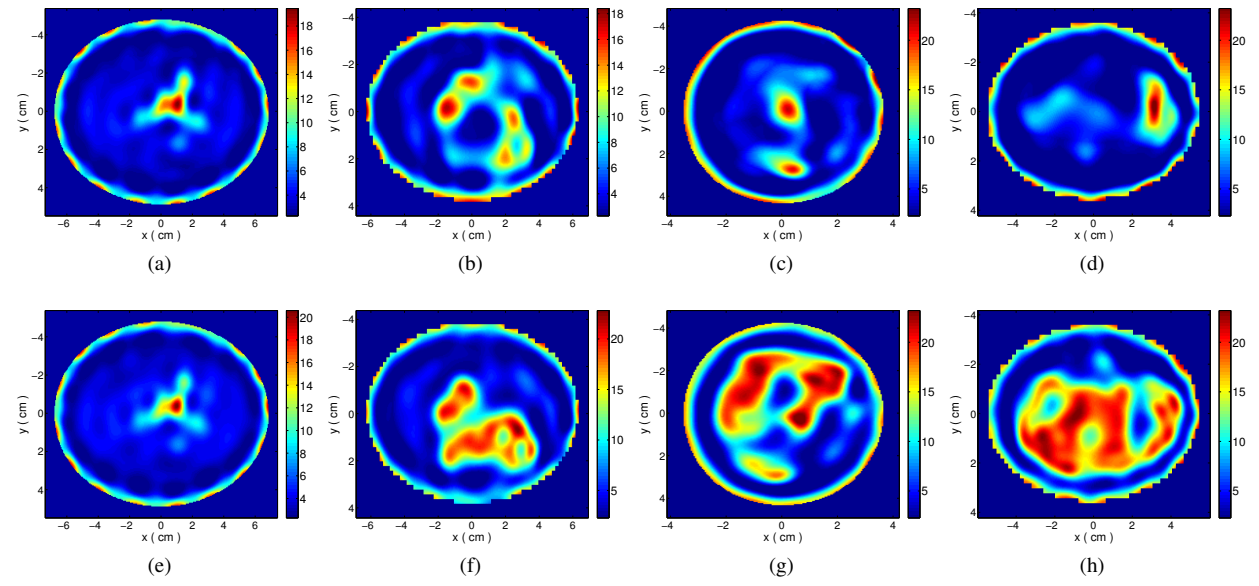

Fig. 8. Reconstructed images of ϵ_∞ without and with an optimized initial guess for 4 phantoms in 0.5 mm. (a)-(d) Reconstructions with a fixed initial guess representative of normal breast tissue average properties ($\epsilon_\infty = 11.27, \Delta\epsilon = 5.51, \sigma_s = 0.0802$); (e)-(h) Reconstruction with an optimized initial guess.

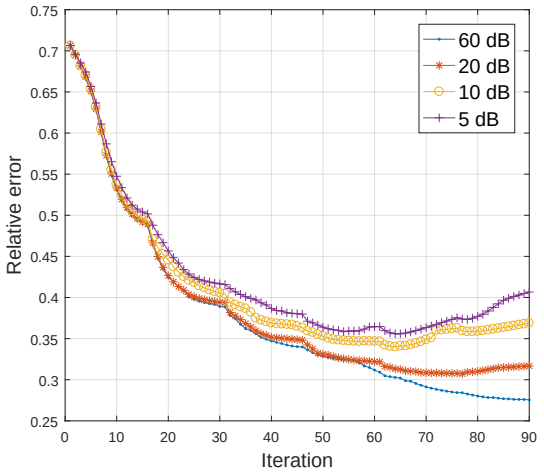

Fig. 9. Comparison of reconstruction quality for different SNR levels of noise and phantom '062204'.

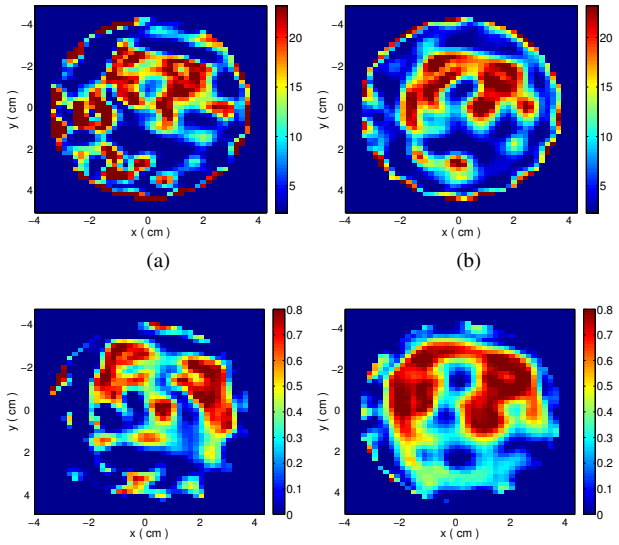

Fig. 10. Reconstructed images of ϵ_∞ and σ_s in 2 mm under 5 dB noise. Top: Estimates of ϵ_∞ without (a) and with (b) L^1 regularization. Bottom: Images of σ_s without (c) and with (d) L^1 regularization.

the difference in the Debye parameters of the fixed initial guess from the true average Debye parameters is the most significant. It is also true for three of the four phantoms in the highest 0.5 mm resolution grid, where the number of unknowns (and thus the degree of ill-posedness of the LIP) increases dramatically relative to the low 2 mm resolution grid. Therefore, optimizing the initial guess can increase the algorithm's robustness and enhance the accuracy of reconstruction in high resolution.

C. L^1 norm regularization effect

In all our previous reconstructions, stability in the DBIM-TwIST algorithm has been achieved by terminating the TwIST iterations based on an adaptive strategy presented in our previous work [10]. Although noise has not been added to the simulated data, this implicit regularization strategy can ensure stability in cases of noise or measurement uncertainties, similar to previous implementations using the CGLS method [6]–[8]. To illustrate this, we have repeated the reconstructions of Section IV-B with an increasing level of noise in the data, and plotted the relative errors to the experimental phantom '062204' in Fig. 9. The plot confirms that convergence is not affected by noise levels with signal to noise ratios (SNRs) as low as 20 dB, but for lower SNRs there is noticeable degradation in the reconstruction quality.

It is important to note that these low SNRs would not correspond to thermal noise in an experimental MWI system, but rather to errors due to measurement uncertainties, environmental factors, and mismatch errors between our model and true experiment. These errors depend on the signal level at each antenna. We have modelled this measurement noise as additive Gaussian in the absence of a better model, with power level dependent on the signal at each antenna. Noise of the same power at each antenna would correspond to thermal noise, which would be well below the level of the signals that are processed by our algorithm and would therefore have a negligible effect in our reconstructions.

To deal with cases of very low SNR where the TwIST termination criterion is not sufficient to guarantee optimal convergence, (10 dB or below in Fig. 9), we can employ the L^1 regularization strategy based on the Pareto curve analysis presented in Section III-C. To illustrate the effect of L^1-regularization approach, we compare in Fig. 10 the reconstructed images of ϵ_∞ and σ_s without and with our L^1 regularization for an SNR of 5 dB. These images demonstrate that our L^1 regularization approach can assist in recovering the true breast composition, while very strong noise artefacts occur when the DBIM-TwIST is implemented without the L^1-regularization correction. As expected, noise artefacts are stronger in the fatty tissue, and affect the σ_s images more than ϵ_∞.

D. Impact of uncertainties in prior information and losses in coupling medium

Our previous reconstructions have assumed prior knowledge of the outer outline of the breast model and a fixed relaxation time for all Debye parameters. Moreover, a hypothetical lossless coupling medium with low dielectric constant has been considered, motivated by the use of low-loss coupling media such as safflower oil. In this section, we consider the impact on the reconstruction due to losses in the coupling medium, as well as the effect of uncertainties in the knowledge of the breast outline and the relaxation constant.

The impact of the coupling medium in microwave breast imaging has been considered in various previous studies, both in radar-based as well as tomographic approaches. For example its effect in terms of signal level has been studied in [30], while the use of losses to reduce unwanted signals in microwave tomography has been demonstrated in [31]. It is evident that a lossy coupling medium will reduce the level of signals scattered by the breast, and this loss of information can affect the quality of reconstructions.

TABLE IV
RELATIVE RECONSTRUCTION ERRORS FOR VARIOUS COUPLING MEDIA AND PHANTOM '062204'

coupling medium	ϵ_∞	$\Delta\epsilon$	σ_s	τ	Relative error
Ideal lossless	2.6	0	0	17.1	0.322
Corn syrup	18.7	0	0.64	13.6	0.698
Triton X-100	3.51	2.58	0.066	41.6	0.415
80% Glycerine	5.73	16.7	0.415	111.1	0.621

TABLE V
RELATIVE RECONSTRUCTION ERRORS FOR PHANTOM '062204' DUE TO UNCERTAINTIES IN THE BREAST OUTLINE

Error of model's dimension		Error of model's position	
model error	Relative error	model error	Relative error
2.67%	0.376	5.65%	0.450
8.40%	0.450	8.84%	0.544
15.97%	0.430	16.05%	0.597

TABLE VI
RELATIVE RECONSTRUCTION ERRORS FOR PHANTOM '062204' DUE TO VARIOUS BIASES OF τ

Precise relaxation time		Relative error		
coupling medium	$\tau(ps)$	1%	5%	10%
Ideal lossless	17.1	0.3776	0.3789	0.377

Table IV quantifies the effect of considering some commonly used lossy coupling media, such as corn syrup, Triton X-100, and 80% glycerine. We employ corn syrup Sample 1 from [32], and the data of the Triton X-100, and 80% glycerine are based on our own measurements. It is evident that a higher conductivity in the coupling medium leads to less accurate reconstructed images due to the additional signal loss. This was confirmed by performing additional reconstructions for hypothetical media with the same dielectric constants as in Table IV but without losses, where no degradation in quality was observed.

As it may be impossible to have exact knowledge of the outer outline of the breast model in a practical experiment, we performed an error level analysis for uncertainties in the position and size of the breast structure, presented in Table V. Reconstructions with uncertainties in the assumed breast size and position have been analysed separately and their errors are calculated in this table. The relative reconstruction error is not affected significantly by uncertainties in the breast size, but misalignments of the assumed breast outline from the true position affect the reconstruction quality only for over a 8% error. These results suggest that the algorithm is robust with respect to uncertainties in the knowledge of the breast shape.

Finally, we also examined the impact of performing reconstructions with a relaxation time τ, which is different from the assumed value of 17.125 ps for the breast tissue Debye models by a variation of up to 10%. Our results in Table V remain unaffected by this mismatch in the assumed model, producing visually similar images and relative error with a maximum variation of 1%.

V. CONCLUSION

We presented a novel multiple frequency DBIM algorithm for microwave breast imaging based on the TwIST method. We have argued that this implementation is more flexible and robust than the CGLS method as a solver of the ill-posed linear problem. By using a hybrid multi-frequency approach, we have achieved an optimal trade-off between imaging accuracy and reconstruction stability for this method. We also proposed a new approach to obtain an optimized initial guess of the average breast tissues properties by sampling along the range of possible values and running a few DBIM iterations to find the minimum error. We have also performed reconstructions in multiple resolutions to examine the benefits of our optimization strategies. This allowed us to argue that the optimized initial guess can be obtained in low resolution grids, and that this step prior to estimating the true distributions is essential in order to minimize relative reconstruction errors, especially in high resolutions grids where the number of unknowns increases dramatically.

Moreover, we proposed a new regularization strategy for the TwIST method based on the L^1 norm and the Pareto curve. This optimized regularization approach can guarantee the stability of the imaging system in cases of very high mismatch between our forward model and the experimental system. Finally, we have presented reconstructions for four phantoms of different breast composition, and demonstrated the algorithms robustness with respect to uncertainties in the assumed prior information, namely the breast outline and the value of the relaxation parameter in the tissue Debye models.

Future work will focus on extending this study for three-dimensional geometries, as well as validating the algorithm with experimental data.

REFERENCES

[1] S. Semenov, "Microwave tomography: review of the progress towards clinical applications," *Philosophical Transactions of the Royal Society A: Mathematical, Physical and Engineering Sciences*, vol. 367, no. 1900, pp. 3021–3042, 2009.

[2] Winters *et al.*, "Three-dimensional microwave breast imaging: Dispersive dielectric properties estimation using patient-specific basis functions," *IEEE Trans. Med. Imag.*, vol. 28, no. 7, pp. 969–981, 2009.

[3] C. Gilmore *et al.*, "Microwave biomedical data inversion using the finite-difference contrast source inversion method," *IEEE Trans. Antennas Propag.*, vol. 57, no. 5, pp. 1528–1538, 2009.

[4] R. Scapaticci *et al.*, "Wavelet-based adaptive multiresolution inversion for quantitative microwave imaging of breast tissues," *IEEE Trans. Antennas Propag.*, vol. 60, no. 8, pp. 3717–3726, 2012.

[5] P. M. Meaney *et al.*, "Initial clinical experience with microwave breast imaging in women with normal mammography," *Academic Radiology*, vol. 14, no. 2, pp. 207 – 218, 2007.

[6] J. D. Shea *et al.*, "Three-dimensional microwave imaging of realistic numerical breast phantoms via a multiple-frequency inverse scattering technique," *Medical Physics*, vol. 37, no. 8, pp. 4210–4226, 2010.

[7] P. Kosmas *et al.*, "Three-dimensional microwave imaging of realistic breast phantoms via an inexact gauss-newton algorithm," in *2008 IEEE Antennas and Propagation Society International Symposium*, 2008, pp. 1–4.

[8] M. Azghani *et al.*, "Microwave medical imaging based on sparsity and an iterative method with adaptive thresholding," *IEEE Trans. Med. Imag.*, 2015.

[9] J. Bioucas-Dias *et al.*, "A new twist: Two-step iterative shrinkage/thresholding algorithms for image restoration," *IEEE Trans. Image Process.*, 2007.

[10] Z. Miao and P. Kosmas, "Microwave breast imaging based on an optimized two-step iterative shrinkage/thresholding method," in *Antennas and Propagation (EuCAP), 2015 9th European Conference on*, 2015, pp. 1–4.

[11] F. Gao *et al.*, "Sensitivity of the distorted born iterative method to the initial guess in microwave breast imaging," *IEEE Trans. Antennas Propag.*, vol. 63, no. 8, pp. 3540–3547, 2015.

[12] T. Grzegorczyk *et al.*, "Fast 3-d tomographic microwave imaging for breast cancer detection," *IEEE Trans. Med. Imag.*, vol. 31, no. 8, pp. 1584–1592, Aug 2012.

[13] T. Isernia *et al.*, "On the local minima in a tomographic imaging technique," *IEEE Trans. Geosci. Remote Sens.*, vol. 39, no. 7, pp. 1596–1607, Jul 2001.

[14] W. C. Chew, *Waves and fields in inhomogeneous media*. IEEE press New York, 1995, vol. 522.

[15] A. Borsic *et al.*, "In vivo impedance imaging with total variation regularization," *IEEE Trans. Med. Imag.*, vol. 29, no. 1, pp. 44–54, Jan 2010.

[16] J. Nasehi Tehrani *et al.*, "A comparison between compressed sensing algorithms in electrical impedance tomography," in *Engineering in Medicine and Biology Society (EMBC), 2010 Annual International Conference of the IEEE*, Aug 2010, pp. 3109–3112.

[17] R. K. Amineh *et al.*, "Three-dimensional near-field microwave holography using reflected and transmitted signals," *IEEE Trans. on Antennas Propag.*, vol. 59, no. 12, pp. 4777–4789, Dec 2011.

[18] M. H. Bakr and N. K. Nikolova, "An adjoint variable method for time domain tlm with fixed structured grids," in *IEEE MTT-S International Microwave Symposium Digest, 2003*, vol. 2, June 2003, pp. 1121–1124 vol.2.

[19] C. Gilmore *et al.*, "A wideband microwave tomography system with a novel frequency selection procedure," *IEEE Transactions on Biomedical Engineering*, vol. 57, no. 4, pp. 894–904, April 2010.

[20] W. Chew and J. Lin, "A frequency-hopping approach for microwave imaging of large inhomogeneous bodies," *Microwave and Guided Wave Letters, IEEE*, vol. 5, no. 12, pp. 439–441, Dec 1995.

[21] D. M. Young, *Iterative solution of large linear systems*. Elsevier, 2014.

[22] M. Azghani and F. Marvasti, "Iterative methods for random sampling and compressed sensing recovery," in *Sampling Theory and Applications. Proceedings of 10th International Conference on Eurasip*, 2013.

[23] O. Axelsson, *Iterative solution methods*. Cambridge University Press, 1996.

[24] T. Blumensath and M. E. Davies, "Iterative thresholding for sparse approximations," *Journal of Fourier Analysis and Applications*, vol. 14, no. 5-6, pp. 629–654, 2008.

[25] R. Scapaticci *et al.*, "Wavelet-based regularization for robust microwave imaging in medical applications," *IEEE Trans. Biomed. Eng.*, vol. 62, no. 4, pp. 1195–1202, April 2015.

[26] E. Zastrow *et al.*, "Development of anatomically realistic numerical breast phantoms with accurate dielectric properties for modeling microwave interactions with the human breast," *IEEE Trans. Biomed. Eng.*, vol. 55, no. 12, pp. 2792–2800, Dec 2008.

[27] O. Bucci and T. Isernia, "Electromagnetic inverse scattering: Retrievable information and measurement strategies," *Radio Science*, vol. 32, no. 6, pp. 2123–2137, 1997.

[28] S. S. Chen *et al.*, "Atomic decomposition by basis pursuit," *SIAM journal on scientific computing*, vol. 20, no. 1, pp. 33–61, 1998.

[29] C.R.Vogel, "Non-convergence of the l-curve regularization parameter selection method," *Inverse problems*, vol. 12, no. 4, p. 535, 1996.

[30] P. Kosmas, C. M. Rappaport, and E. Bishop, "Modeling with the fdtd method for microwave breast cancer detection," *IEEE Trans. Microw. Theory Tech.*, vol. 52, no. 8, pp. 1890–1897, 2004.

[31] G. Colin *et al.*, "A study of matching fluid loss in a biomedical microwave tomography system," *Medical Physics*, vol. 40, no. 2, pp. 023 101–n/a, 2013.

[32] G. Bindu *et al.*, "Dielectric studies of corn syrup for applications in microwave breast imaging," *Progress In Electromagnetics Research*, vol. 59, pp. 175–186, 2006.

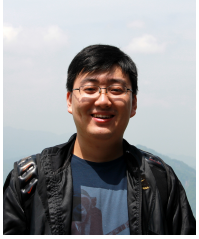

Zhenzhuang Miao received the bachelor's degree in telecommunication engineering from University of Science and Technology Beijing in 2010 and the master degree in electronic engineering with business management from King's College London. Since 2013, his scientific research interests are mainly focused on microwave imaging based on tomographic method, inverse problems techniques, ill-posed linear problems for breast cancer detection and regularization method for the microwave imaging.

Dr. Panagiotis Kosmas (M'05-SM'14) received the Diploma in Electrical and Computer Engineering from the National Technical University of Athens, Greece, in 1999, and the M.S. and Ph.D. degrees in Electrical and Computer Engineering from Northeastern University, Boston, MA, in 2002 and 2005, respectively. He joined Kings College London (KCL) in 2008 as a Lecturer, and is currently a Senior Lecturer at KCLs Department of Informatics. Prior to his appointment at KCL, he held research positions at the Center for Subsurface Sensing and Imaging Systems, Boston, USA, the University of Loughborough, UK, and the Computational Electromagnetics Group, University of Wisconsin-Madison, USA. He is also a co-founder of Mediwise Ltd, an award-winning UK-based SME focusing on the use of electromagnetic waves for medical applications. He is an elected Working Group leader for COST Action MiMed (TD1301), Development of a European-based Collaborative Network to Accelerate Technological, Clinical and Commercialisation Progress in the Area of Medical Microwave Imaging. His research interests include computational electromagnetics with application to sensing and imaging, antenna design, physics-based detection methods, and inverse problems theory and techniques.